Biosensors and Bioelectronics 186 (2021) 113283

Contents lists available at ScienceDirect

Biosensors and Bioelectronics

journal homepage: www.elsevier.com/locate/bios

Short communication

Design and development of ferrocene-containing chitosan-cografted-branched polyethylenimine redox conjugates for monitoring free flap failure after reconstructive surgery

Lu Gan [a], Fiona Wei Ling Loke [b], Wai Chye Cheong [b], John Shen Him Ng [b], Ngian Chye Tan [a], Zanzan Zhu [b,*]

[a] Division of Surgical Oncology, National Cancer Centre Singapore, 11 Hospital Crescent, 169610, Singapore
[b] Medical Technology Office, SingHealth, 20 College Road, Academia, 169856, Singapore

ARTICLE INFO

Keywords:
Ferrocene-containing redox polymers
Continuously metabolites monitoring
Free flap
Electrochemical biosensor

ABSTRACT

We reported a proof-of-concept study of developing an electrochemical biosensor for prolonged continuous monitoring free flap failure caused by vascular occlusion after reconstructive surgery. Ferrocene (Fc)-containing Chitosan-cografted-Branched Polyethylenimine redox conjugates (CHIT-Fc-co-BPEI-Fc) were used as pH-tuneable matrix to attach the target enzymes (glucose oxidase ≡ GOD and lactate oxidase ≡ LOD, respectively) to build up the corresponding GOD-sensor and LOD-sensor. The sensitivity of GOD-/LOD-sensor was found to be 2.89(±0.06)μA/mM and 2.95(±0.19)μA/mM with a limit of detection (*LOD*) of 0.047 mM and 0.172 mM, respectively. The sensor performance was further pre-clinically validated via rabbit study, which confirmed that the designed biosensors could electrochemically detect the changes of metabolite levels caused by flap failure within minutes. This sensor protocol is able to be fabricated as embedded biosensor for prolong continuous detection for clinical application/research.

1. Introduction

Free flap surgery refers to the transfer of patients' own well-vascularized tissue from a healthy site to a defect site (McCarty et al., 2019), then blood supply is reconstructed at the defect site via microsurgical techniques (Cervenka and Bewley, 2015). Although most studies have found that the success rate of free flap transfer varies between 95% and 97% (Agrawal et al., 2015; Jeng et al., 2012), practically its failure still exists and remains a challenge for both surgeons and patients (Colak et al., 2018). The majority of flap failures are caused by vascular thrombosis and occur within the first 48 h after reconstructions (Novakovic et al., 2009). The early detection of vascular thrombosis is considered the key to decrease flap failure rate and enhance salvage rate (Kagaya et al., 2017; Chao and Lamp, 2014). Clinical monitoring based on subjective criteria (such as skin colour, temperature, skin turgor and capillary refill time) remains the gold standard of postoperative monitoring of free flap, but the results are unreliable because such method is highly observer-dependent (Cervenka and Bewley, 2015). Many technologies have been proposed and developed to detect early vascular thrombosis for free flap postoperative monitoring, while so far there is no universally accepted method (Chao and Lamp, 2014). These technologies vary in monitoring mechanisms, invasiveness, cost, feasibility and relative efficacy (Kohlert et al., 2019). For instance, Doppler technology is used to monitor free flap failure via measuring the vascular flow in free flaps (Colak et al., 2018). However, hand-held Doppler is difficult for surgeons to target the right vessel to monitor (Devine et al., 2001), while the implantable Doppler suffers from a high false-positive rate (Kohlert et al., 2019; Chen et al., 2016). The near-infrared spectroscopy and microdialysis are applied to monitor free flap through detecting the tissue metabolism and ischemia (Colak et al., 2018; Chen et al., 2016). The former technique continuously studies tissue perfusion and oxygenation in free flaps by near-infrared wavelengths, the whole detection process is high cost. Microdialysis measures the concentration of anaerobic metabolites in free flaps and can achieve early detection of flap failure, but it suffers from high cost and false-positive rate.

Inspired by previous studies that the on-set of ischemia by vascular compromise/occlusion can be detected from changes in glucose level (decrease) and/or lactate level (increase) (Karakawa et al., 2018), in this

* Corresponding author.
E-mail address: zhu.zan.zan@singhealth.com.sg (Z. Zhu).

https://doi.org/10.1016/j.bios.2021.113283
Received 16 February 2021; Received in revised form 6 April 2021; Accepted 22 April 2021
Available online 30 April 2021

study, electrochemical technology is applied to monitor the tissue metabolism to judge the flap failure. Comparing to all those monitoring technologies mentioned above, the electrochemical biosensor is rapid, robust, stable, accurate, portable and easy to miniaturize or multiplex involving low production cost only. To develop the electrochemical biosensor, a ferrocene (Fc)-containing chitosan-cografted-branched polyethylenimine (CHIT-Fc-co-BPEI-Fc) redox conjugate is designed (Scheme 1). Such redox conjugate acts as a biocompatible polymer matrix to immobilize the glucose oxidase (GOD) and lactate oxidase (LOD) onto electrodes. The proof-of-concept study was successfully conducted in animal model, wherein the flap failure was mimicked by manually operating the vascular occlusion.

2. Results and discussion

2.1. Design of redox conjugates CHIT-$Fc_{0.4}$-co-BPEI-$Fc_{0.5}$

Chitosan (CHIT) and branched polyethylenimine (BPEI) are popular candidates for biosensor fabrication (Casadidio et al., 2019; Zakeri et al., 2018). CHIT is well-known to form a hydrophilic film with strong-adhesion ability in buffer solution but it has low electron transfer efficiency. The use of a redox mediator (Fc) is critical to the electrical communication with the enzymes' deeply embedded active sites (Hecht et al., 1993). Covalent linking of the Fc group to CHIT and BPEI can prevent its leakage, while enjoying a good electron transfer efficiency. Individually applying CHIT-Fc or BPEI-Fc as the redox polymer matrix for enzyme attachment suffered different drawbacks: CHIT-Fc has good solubility in acid solution (pH 2.5–3.5), while such low pH environment is not friendly to enzyme's bioactivity. BPEI-Fc could provide a more alkaline pH environment (pH 8.0–9.0); however, it is easy to dissolve in buffer solution during the test, causing poor adhesion to electrode surface. Herein, we use a method that could be applied in scale-up manufacturing to combine CHIT-Fc and BPEI-Fc redox components together under room temperature: via a widely used crosslinker, glutaraldehyde (GA) (Li et al., 2017). This cografted conjugate can balance the polymer's intrinsic pH with the good adhesion requirements: the high hydrophilic nature of BPEI enables a good solubility of CHIT-Fc-co-BPEI-Fc at physiological pH, and CHIT ensures a strong adhesion of the polymer film to electrode surface.

Herein, ferrocenecarboxylic acid was reacted to CHIT with 40% w/w grafting ratio (denoted as CHIT-$Fc_{0.4}$) and chlorocarbonyl ferrocene was reacted to BPEI with 50% w/w grafting ratio (denoted as BPEI-$Fc_{0.5}$). Experimental details can be found in Supplemental Information (**SI**). The successful attachment of Fc group to CHIT and BPEI was proved by gel permeation chromatography (GPC) analysis (Gan et al., 2018) (Fig. 1a): comparing to pure CHIT and BPEI, the UV absorbance peak at 440 nm (characteristic peak of Fc) were all found in CHIT-$Fc_{0.4}$, BPEI-$Fc_{0.5}$ and CHIT-$Fc_{0.4}$-co-BPEI-$Fc_{0.5}$. The higher UV absorbance of the cografted conjugates attributed to the more Fc moieties than the individual components. The cografted conjugates indicated earlier refractive index (RI) peak due to its larger molecular weight. The thickness of the single polymer film layer was examined to be 2.5 (±0.3)μm (Fig. 1c–e).

2.2. Cyclic voltammetry (CV) study of redox conjugates CHIT-$Fc_{0.4}$-co-BPEI-$Fc_{0.5}$

In order to investigate the electrochemical activity of CHIT-$Fc_{0.4}$-co-BPEI-$Fc_{0.5}$ conjugates, CV experiments were performed in 1X PBS buffer from negative potential to positive side, setting redox components CHIT-$Fc_{0.4}$ and BPEI-$Fc_{0.5}$ as references. As seen in Fig. 1b, CV results indicated that Fc retained its electrocatalytic activity in immobilized form, wherein CHIT-$Fc_{0.4}$ and BPEI-$Fc_{0.5}$ displayed the oxidation potential, E_{pa1} at 0.42 V, and E_{pa2} at 0.30 V, respectively. Lower oxidation potential was found in BPEI-$Fc_{0.5}$ than CHIT-$Fc_{0.5}$ because branch polymer provides more flexible backbone/side chains, promoting faster/easier

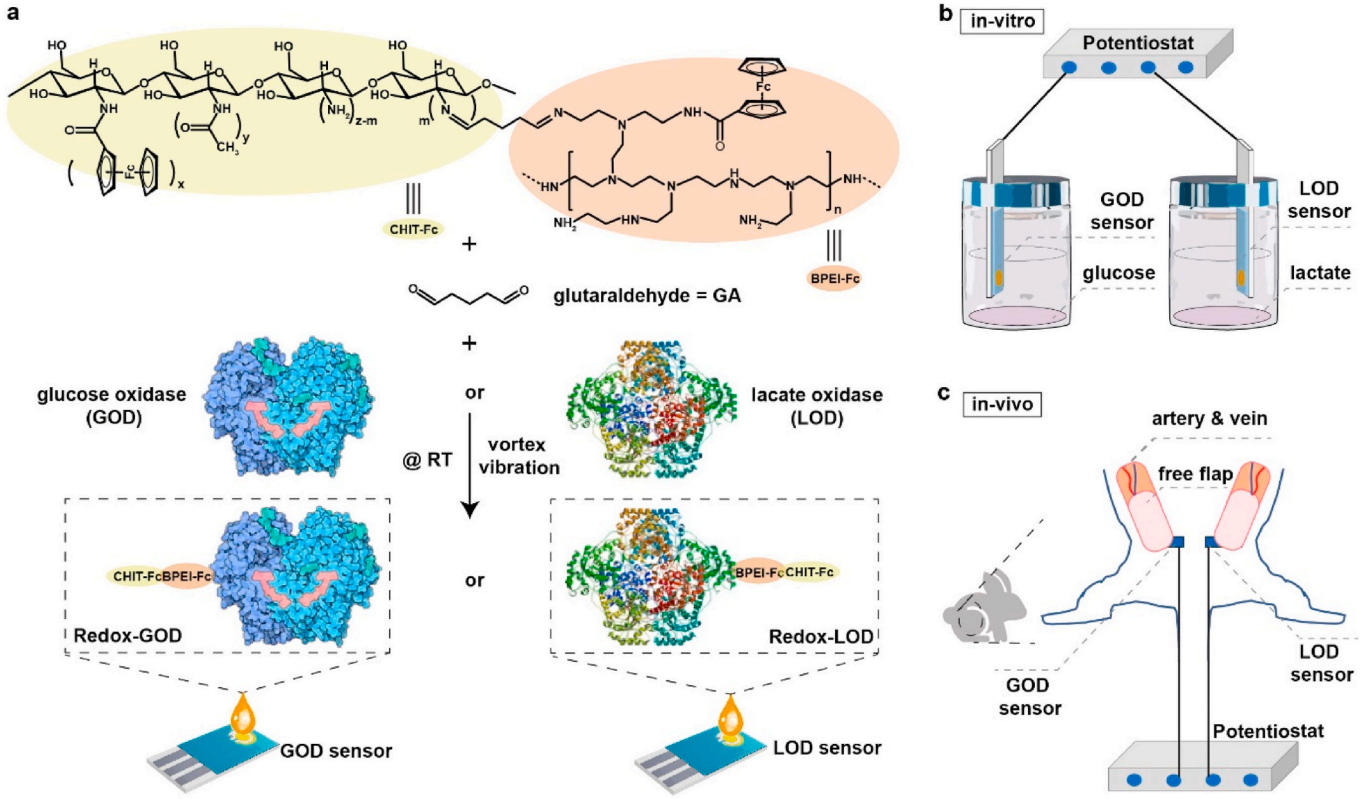

Scheme 1. (a) Synthesis steps of enzymes attaching to designed cografted redox conjugates with the present of glutaraldehyde as crosslinker. (b) Electrochemical performance of GOD-sensor and LOD-sensor was tested *in-vitro*, separately. (c) Illustration of *in-vivo* sensor testing.

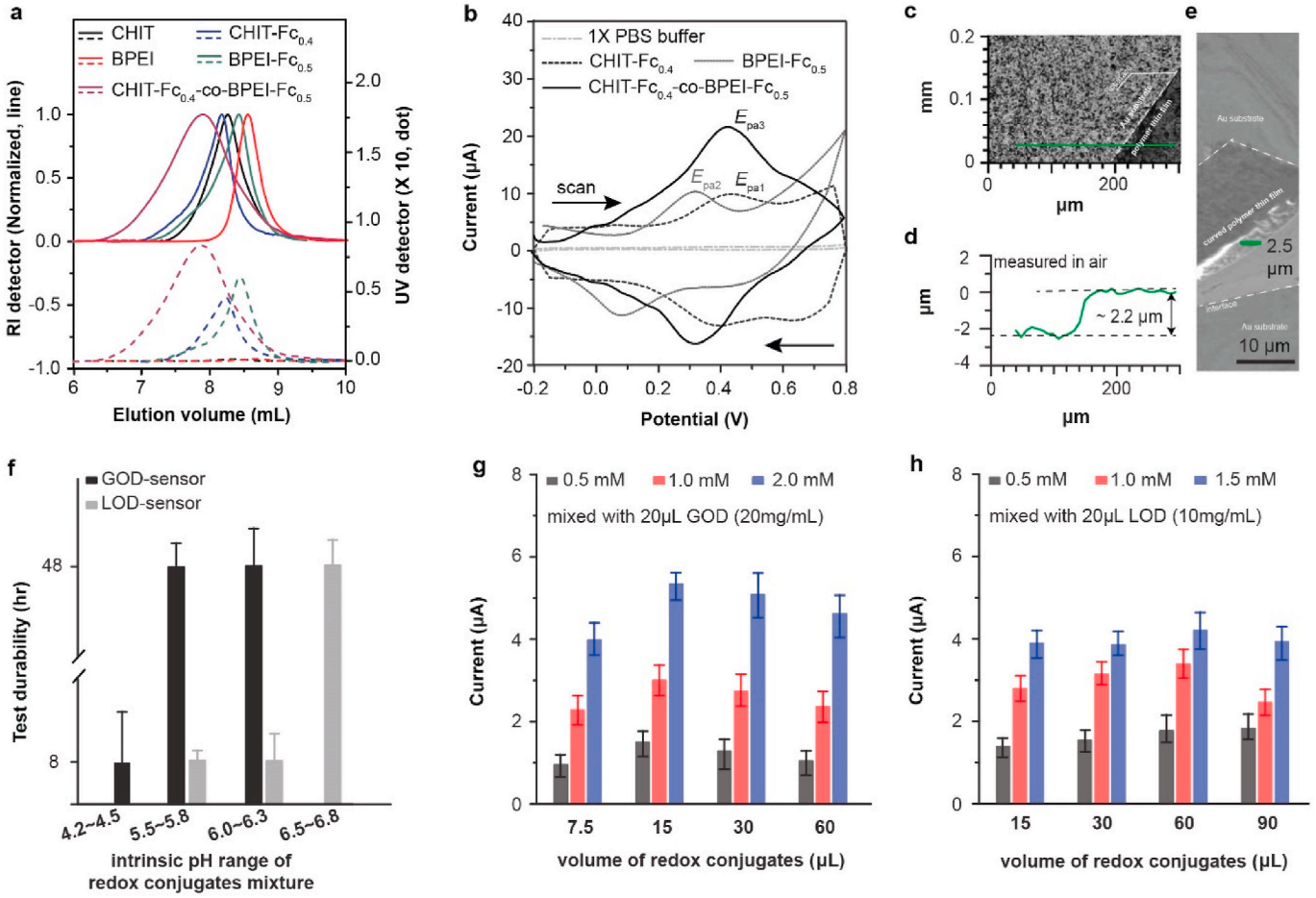

Fig. 1. (a) GPC signals measured for CHIT and BPEI (as control), CHIT-$Fc_{0.4}$, BPEI-$Fc_{0.5}$ and CHIT-$Fc_{0.4}$-co-BPEI-$Fc_{0.5}$ cografted conjugates. RI analysis (after normalization) was indicated in solid lines, UV absorbance (× 10) at 440 nm was indicated in dot lines. (b) CV of CHIT-$Fc_{0.4}$, BPEI-$Fc_{0.5}$ and CHIT-$Fc_{0.4}$-co-BPEI-$Fc_{0.5}$ conjugates. The test buffer was 1X PBS (pH 7.2) and the scan rate was 100 mV/s. (c) Microscope image of exposed Au surface and the scratched polymer thin film. Dash line indicates the Au/polymer film interface. (d) Thickness profile analysis (measured in air) by optical surface profiler for polymer film showed in (c). (e) Cross-section scanning electron microscope of the curved polymer thin film. Dash line indicates the Au/polymer film interface. (f) Intrinsic pH effect of redox conjugate mixture on sensor testing durability. (g) Optimization of volume of CHIT-$Fc_{0.4}$-co-BPEI-$Fc_{0.5}$ redox conjugates to certain amount of GOD. The amperometric response current was recorded (in 1X PBS, pH 7.2) at glucose concentration: 0.5 mM, 1.0 mM and 2.0 mM, respectively. (h) Optimization of volume of CHIT-$Fc_{0.4}$-co-BPEI-$Fc_{0.5}$ redox conjugates to certain amount of LOD. The amperometric response current was recorded (in 1X PBS, pH 7.2) at sodium lactate concentration: 0.5 mM, 1.0 mM and 1.5 mM, respectively.

electron transfers. E_{pa3} of CHIT-$Fc_{0.4}$-co-BPEI-$Fc_{0.5}$ conjugates occurred at 0.40 V, indicating the neutralized oxidation potential from individual redox components.

2.3. *Effect of the intrinsic pH of redox conjugate mixture and the redox conjugate-to-enzyme ratio*

To optimize the sensor performance, we have optimized the redox-enzyme formulations from two aspects: firstly, the ratio between two redox components (*i.e.*, CHIT-$Fc_{0.4}$ and BPEI-$Fc_{0.5}$) was regulated to adjust the intrinsic pH of redox conjugate mixture (Fig. 1h). We have found that the intrinsic pH of redox conjugate mixture obviously influenced the sensor testing durability: the durability of GOD-sensor was significantly extended if mixing with redox conjugates in less acidic pH (pH 5.5–6.0). However, LOD-sensor's performance was better when mixing with redox conjugates in pH 6.5. The reported optimum pH range for the free and immobilized LOD is 6.0–7.0 (Hajizadeh et al., 1991; Duncan et al., 1989), when the intrinsic pH of the redox matrix is sufficiently mild to permit retention of enzymatic activity and stability, the enzymatic reaction should retain persistence (Stoisser et al., 2016). Hence, we have inferred that LOD gradually diminished its stability and activity when mixing with redox conjugates in pH below 6.5 so that the sensor failed after several hours testing. These finding are in agreement with the previous studies by Huang et al. (2007) on sol-gel film-based L-lactate biosensor, where at sol-gel film pH about 6.5, the sensor displayed the optimized performance. In this work, an optimized intrinsic pH of redox conjugate mixture, pH 6.0 and pH 6.5, was selected to fabricate GOD- and LOD-sensor, respectively, to achieve at least 60 h continuous sensing. In *in-vitro* evaluation, all fabricated sensors were immersed into 1X PBS (pH 7.2) to mimic the normal physiological pH. Secondly, the ratio of redox conjugate-to-enzyme was optimized by adding different volume of redox conjugates to certain volume of enzymes (Fig. 1f–g). We concluded that the redox conjugate-to-enzyme ratio slightly affected the steady-state current value: when sensing glucose at 0.5 mM, 1.0 mM and 2.0 mM, 15 μL redox conjugates mixing with 20 μL GOD provided the best current response for GOD-sensor; for LOD-sensor, when sensing sodium lactate at 0.5 mM, 1.0 mM and 1.5 mM, 60 μL redox conjugates provided the slightly better current response, while the other ratios displayed approximative values. This result suggested the saturated ratio between redox conjugates to GOD was 3:4 and to LOD was 3:1, respectively.

2.4. In-vitro evaluation of the sensor

To mimic the metabolite changes upon flap failure, *in-vitro* current response of GOD/LOD-sensor was continuously investigated at room temperature in glucose and sodium lactate solution (under stirring) over 60h, respectively and separately (Scheme 1b). After reaching a steady-state background current, an aliquot of glucose or sodium lactate at known concentration was added into PBS buffer (pH 7.2) solution every 60s–180s under continuously stirring. Typical amperometric responses of GOD-/LOD-sensor with successive addition of glucose and sodium lactate are displayed in Fig. 2a and Fig. 2d, respectively. The sensors performed fast response (~5s) to achieve steady-state current, the current increased as a function of time and eventually reached a limiting value. The corresponding linear calibration curve (Fig. 2b and e) indicated the sensor's sensitivity was 2.89(±0.06)μA/mM and 2.95(±0.19)μA/mM, for GOD- and LOD-sensor, respectively. However, the sensitivity of both sensors slowly and gradually decreased upon continuously sensing up to 60 h (Fig. 2c and f). For GOD-sensor, the linear dynamic detection range was 0.05–2.0 mM and was up to 1.5 mM for LOD sensor. Furthermore, enzyme–substrate kinetics for the biosensor was investigated by the Michaelis−Menten kinetics, which can be written according to the Lineweaver–Burk equation $1/J_{ss} = 1/J_{max} + (K_M^{'}/J_{ss})(1/C)$ where J_{ss}, J_{max}, $K_M^{'}$ and C are the steady state current, the maximum response current, the apparent Michaelis constant of the electrode, and the substrate concentration, respectively. The driven $K_M^{'}$ was 1.55 mM for GOD-sensor, and 6.88 mM for LOD-sensor, respectively (Fig. S3). The limit of detection (*LOD*) and limit of quantitation (*LOQ*) are estimated via Linear Regression model, expresses as $LOD = 3S_a/b$, and $LOQ = 10S_a/b$, respectively, where S_a is the standard deviation of intercepts of regression lines and b is the slope of the calibration curve. Here, GOD-/

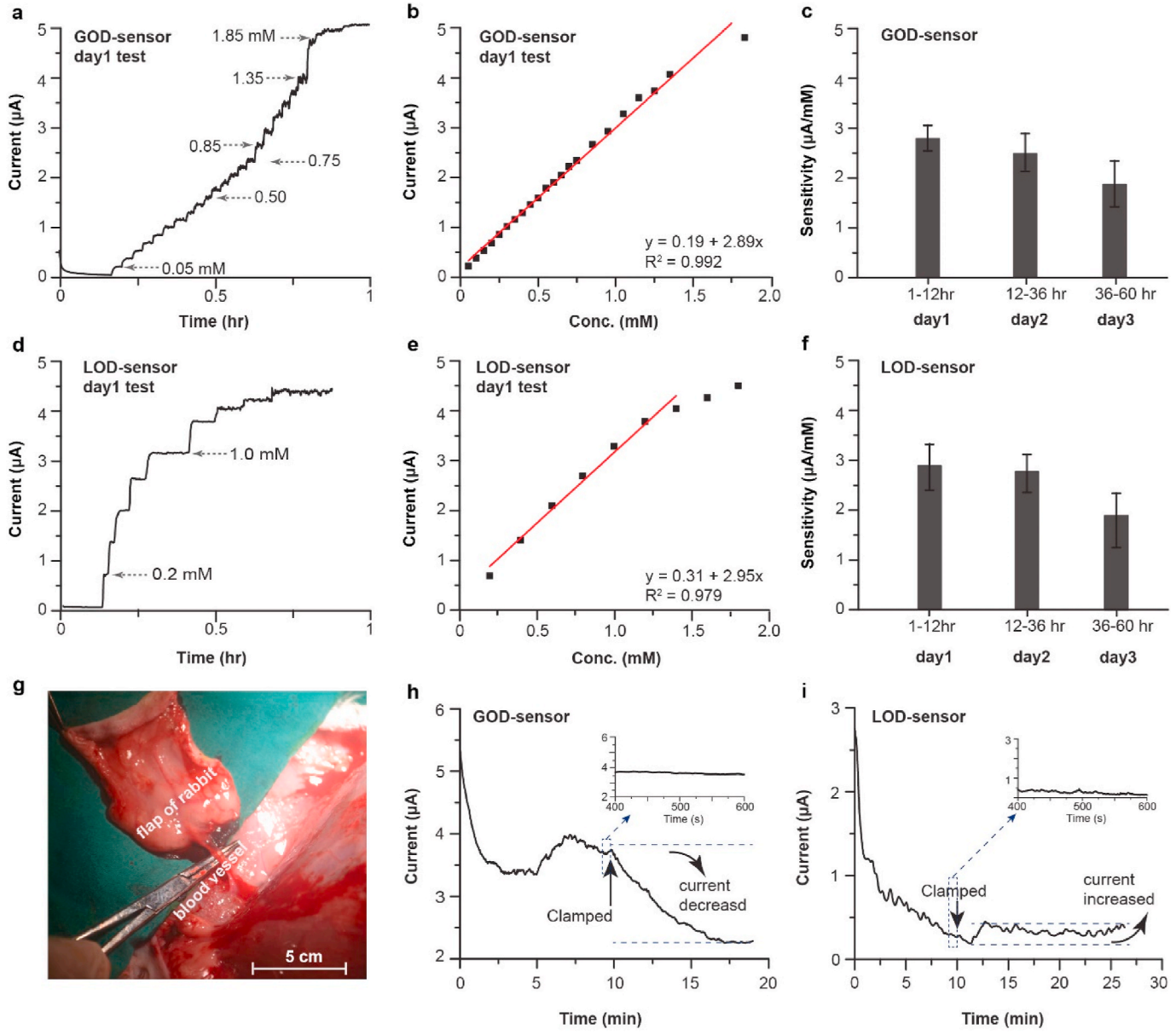

Fig. 2. (a) i-t curve obtained by GOD-senor upon successive addition of aliquots of glucose solution to 20 mL of stirred 1X PBS (pH 7.2). (b) Calibration curve of GOD-sensor according to i-t test in (a). (c) Sensitivity of GOD-sensor as the function of test durability. (d) i-t curve obtained by LOD-senor upon successive addition of aliquots of sodium lactate solution to 20 mL of stirred 1X PBS (pH 7.2). (e) Calibration curve of LOD-sensor according to i-t test in (d). (f) Sensitivity of LOD-sensor as the function of test durability. (g) The image of free flaps of rabbit. (h) i-t test of GOD-sensor on rabbit free flap. (i) i-t test of LOD-sensor on rabbit free flap. The inset figures in (h) and (i) indicate the ~3min stabilizing baseline current before clamping. Dash lines are guide for eyes. The applied potential for all the i-t test was 0.5 V and the *in-vitro* test was conducted at room temperature.

LOD-sensor obtained a *LOD* of 0.047 mM and 0.172 mM, respectively, and a *LOQ* of 0.157 mM and 0.572 mM, respectively.

2.5. In-vivo evaluation of the sensor

To investigate the designed biosensors in animal model, vessel occlusion was mimicked by cutting off the blood supply of free flaps. The experiment protocol was reviewed and approved by SingHealth Institutional Animal Care and Use Committee. The animal trial complied with the National Advisory Committee for Laboratory Animal Research guidelines. A 3 kg New Zealand white female rabbit was selected for the study. The rabbit was housed in the animal facility at SingHealth Experimental Medicine Centre. All surgeries were performed under general anesthesia and aseptic conditions using sterile surgical instruments. Bilateral skin flaps were raised on the abdomen of the rabbit and were islanded based on blood supply from the inferior epigastric vessels on each side of the rabbit. To monitor the glucose and lactate levels of the flaps, glucose sensor and lactate sensor was attached on each flap, respectively.

As shown in the Fig. 2h-i, occlusion of the blood vessel was performed at the 10th min for both sensors. A significant drop in current was observed for the glucose sensor almost immediately after clamping vessel. The current decreased from original 3.75 μA to end up at 2.25 μA, approximately 40% current decrease was observed in 8mins. For the lactate sensor, an increase in current was observed at the 12th min, 4mins after the vessel occlusion of the flap. The current increased from 0.17 μA to 0.31 μA, approximately 80% current increase was observed at the 13th min. The delay in the current response may be caused by the slow accumulation of lactate in the skin flap after the occlusion. The *in-vivo* trial results confirmed that the developed biosensor is able to electrochemically detect the changes of metabolite levels caused by flap failure within minutes. In this proof-of-concept study, due to the limited size of the rabbit, there were no control flaps raised in the *in-vivo* trial, a "relative current" value is clear to indicate the change of metabolite level. More comprehensive evaluations will be conducted in our following animal studies.

3. Conclusion

In this work, we reported the development and pre-clinical validation of a highly sensitive biosensor for continuous free flap monitoring over a prolonged sensing duration. The proof-of-concept tests indicated the biosensors are promising to continuously monitor the changes of metabolite level in reconstructive flaps. The *in-vitro* study indicated that the sensitivity of GOD-/LOD-sensor was 2.89(±0.06)μA/mM and 2.95 (±0.19)μA/mM with a limit of detection (LOD) of 0.047 mM and 0.172 mM, respectively. In animal study, the designed biosensors successfully detected the flap failure within minutes: a "relative current" change indicated the change of metabolite level. Multiple animal studies will be conducted to evaluate the effectiveness and the stability of the sensors, where pig (genetically closer to human and larger size) will be applied instead of rabbit. The following animal trials will include non-survival and survival studies. Furthermore, the commercial screen-printed-electrode chips will be replaced by a customized biocompatible chip for further *in-vitro* and *in-vivo* studies. Our long-term goal is to develop an automated continuous free flap monitoring detector for better patient care.

Declaration of competing interest

The authors declare that they have no known competing financial interests or personal relationships that could have appeared to influence the work reported in this paper.

Acknowledgement

This work is supported by the grant NRF2017NRF-CG001-003 of the National Research Foundation of Singapore, Central Gap Fund.

Appendix A. Supplementary data

Supplementary data to this article can be found online at https://doi.org/10.1016/j.bios.2021.113283.

Authors' contributions

Zanzan Zhu and Lu Gan contributed to the design of the experiments, data analysis and manuscript preparation. Lu Gan performed the experiments. Ngian Chye Tan performed the *in-vivo* trial. Lu Gan, Zanzan Zhu, and John Ng Shen Him assisted the *in-vivo* trial. Zanzan Zhu, Fiona Loke, Wai Chye Cheong and Ngian Chye Tan contributed to the conception and design of the study.

References

Agrawal, G., Gupta, A., Choudhary, V., Tiwari, S., Verma, K., 2015. Dubey H. Int. Surg. J. 2, 534–538.
Casadidio, C., Peregrina, D.V., Gigliobianco, M.R., Deng, S., Censi, R., Martino, P.D., 2019. Mar. Drugs 17, 369.
Cervenka, B., Bewley, A.F., 2015. Curr. Opin. Otolaryngol. Head Neck Surg. 23, 393–398.
Chao, A.H., Lamp, S., 2014. Plast. Surg. Nurs. 34, 52–56.
Chen, Y., Shen, Z., Shao, Z., Yu, P., Wu, J., 2016. Ann. Plast. Surg. 76, 590–597.
Colak, O., Mutlu, O.O., Ozer, K., 2018. Eur. J. Med. Res. 34, 61–65.
Devine, J.C., Potter, L.A., Magennis, P., Brown, J.S., Vaughan, E.D., 2001. J. Wound Care 10, 525–529.
Duncan, J.D., Wallis, J.O., Azari, M.R., 1989. Biochem. Biophys. Res. Commun. 164, 919–926.
Gan, L., Tan, N.C.S., Shah, A.H., Webster, R.D., Gan, S.L., Steele, T.W.J., 2018. Macromolecules 51, 6661–6672.
Hajizadeh, K., Halsall, H.B., Heineman, W.R., 1991. Talanta 38, 37–47.
Hecht, H.J., Schomburg, D., Kalisz, H., Schmid, R.D., 1993. Biosens. Bioelectron. 8, 197–203.
Huang, J., Song, Z., Li, J., Yang, Y., Shi, H., Wu, B., Anzai, J.I., Osa, T., Chen, Q., 2007. Mater. Sci. Eng. C 27, 29–34.
Jeng, S.F., Tan, N.C., Chang, G., 2012. Med. J. 35, 219–230.
Kagaya, Y., Arikawa, M., Miyamoto, S., 2017. Plast. Reconstr. Surg. Glob. Open. 5, e1446.
Karakawa, R., Yoshimatsu, H., Narushima, M., Iida, T., 2018. Plast. Reconstr. Surg. Glob. Open. 6, e1851.
Kohlert, S., Quimby, A.E., Saman, M., Ducic, Y., 2019. Semin. Plast. Surg. 33, 13–16.
Li, R., An, Q.D., Xiao, Z.Y., Zhai, B., Zhai, S.R., Shi, Z., 2017. RSC Adv. 7, 40227–40236.
McCarty, J.L., Corey, A.S., El-Deiry, M.W., Baddour, H.M., Cavazuti, B.M., Hudgins, P.A., 2019. AJNR Am. J. Neuroradiol. 40, 5–13.
Novakovic, D., Patel, R.S., Goldstein, D.P., Gullane, P.J., 2009. Head Neck Oncol. 1, 33.
Stoisser, T., Brunsteiner, M., Wilson, D.K., Nidetzky, B., 2016. Sci. Rep. 6, 27892.
Zakeri, A., Kouhbanani, M.A.J., Beheshtkhoo, N., Beigi, V., Mousavi, S.M., Hashemi, S.A. R., Zade, A.K., Amani, A.M., Savardashtaki, A., Mirzaei, E., Jahandideh, S., Movahedpour, A., 2018. Nano Rev. Exp. 9, 1488497.